Int. J. Therm. Sci. (1999) 38, 160–174

The deduction of friction-induced temperatures from thermal strain measurements in the dry sliding of metallic pairs

Hisham A. Abdel-Aal*

Department of Mechanical Engineering, The University of North Carolina at Charlotte, Charlotte, NC, 28223, USA

(Received 8 January 1998, accepted 29 September 1998)

Abstract—This paper proposes a procedure for utilising thermal strains as a thermometric means to recover the temperature distribution in tribo-specimens. The procedure is demonstrated in relation to strain data obtained by the analysis of the so-called *Double Exposure Speckle Grams*. Total strain components, are resolved into three elements: elastic, plastic, and thermal. These in turn are used to construct a system of difference equations, the solution of which yields a complete characterisation of the strain fields. Thermal strains are subsequently fed into a look-up table containing the coefficient of thermal expansion for the test material at different temperatures to yield the temperature distribution. The results are validated by comparison with an analytical model and relevant experimental data. © Elsevier, Paris.

strain inversion / inverse heat problems / sliding friction / friction heating / laser speckle / dry sliding temperatures / thermal skin

Résumé — Obtention de la température induite par frottement à partir de mesures de déformation thermique dans le glissement sec de paires métalliques. Cet article propose une prodédure utilisant les déformations thermiques comme moyen thermométrique de détermination de la distribution de température dans les études tribologiques. La procédure utilise les données sur les déformations obtenues à partir d'une méthode «speckel» à double exposition. Les composantes de la déformation totale sont résolues selon les cas : élastique, plastique, thermique. Celles-ci sont alors utilisées pour construire un système d'équations différentielles, dont la résolution conduit à la connaissance complète des champs de déformation. Les déformations thermiques sont ensuite introduites dans une table contenant le coefficient de dilatation thermique du matériau testé, à différentes températures, pour obtenir la distribution de température. Les résultats sont validés par comparaison avec un modèle analytique et des résultats expérimentaux. © Elsevier, Paris.

inversion des déformations/ problème de thermique inverse / frottement par glissement / échauffement par frottement / *speckel* laser / température de glissement sec / température de peau

Nomenclature

DESG	double exposure speckle gram	
E	Young's modulus of elasticity	GPa
M	magnification factor	
T	temperature rise	K
U	speckle displacement	m
Z	distance between the film plate and the analysis screen	m
a	thermal diffusivity	$m^2 \cdot s^{-1}$
d	fringe spacing	m
d_1	thickness of zone 1	m
u	horizontal displacement	m
v	vertical displacement	m
Z_{pmax}	maximum penetration depth of an interfacial temperature pulse	m

Greek symbols

Θ	relative strength of a temperature pulse	
α	coefficient of linear thermal expansion	$mm^{-1} \cdot {}^\circ C^{-1}$
δ	Kroneker delta symbol	
λ	wave length of a laser beam	m
ε^T	total *measured* strain	
ε^e	elastic strain	
ε^P	plastic strain	

* haabdela@mailexcite.com

$\bar{\varepsilon}$ computed total effective strain
ε_{ep} computed equivalent plastic strain
μ Poisson's ratio
σ_e equivalent stress

1. INTRODUCTION

The generation of frictional forces between sliding bodies is fundamentally an energy dissipation mechanism that gives rise to heating effects originating at the sliding interface. The increase in the temperature of the rubbing pair can lead to local softening and melting of the material. Furthermore, temperature-rise affects the oxidation rates, the absorption of gases, and the mechanical properties of the sliding pair. Since the release of heat is basically a quasi-continuous process, temperature gradients will develop in the contacting pair. The highest temperature should occur at the points of heat release at the actual contact interface. For this reason, quantification of temperature development in the immediate contact layer of the rubbing solids is of paramount interest. However, the main techniques used for the measurement of temperatures involves considerable difficulties, and it is still not easy to perform accurate and meaningful measurements of friction-induced temperatures [1].

1.1. Thermo-mechanical events in dry sliding

The sequence of thermal events during sliding is mainly that postulated by *flash temperature theory* introduced by Blok [2–4], and worked out by Jaeger [5] and Archard [6] among others. Flash temperature theory bears on the various 'thermal skin' effects induced by the severe constriction which the flow of frictional heat undergoes when penetrating either rubbing body [6]. These thermal skin effects cause the existence of two temperature components within the rubbing pair. The first is the so-called *flash temperature* which is transient in nature and appears at the interface. The second is the bulk temperature which appears some distance away from the contact surface. With repeated sliding over the same surface, the localised temperature flashes that are generated at the tips of the asperities in the surface atoms deposit a quantum of heat into the asperity surface region. That heat is dissipated, since most of the metals are good thermal conductors. Heat is carried back into the asperity with the bulk of the solid acting as a good heat sink for the frictional heat generated at the interface. Thus after a time, the near surface region becomes heated, and the efficiency of dissipation of heat generated in the asperity is reduced.

Mechanically, on the other hand, tribo-specimens will develop characteristic subsurface regions during sliding. These zones are of interest because their analysis leads to important findings concerning the types of tribo-mechanisms that are operative, and to the reasons for observed wear behaviours. The composition and depth of these characteristic zones may not differ if test conditions are identical for two identical specimens. In contrast, for different materials subject to different test parameters, essentially the same zones may still be identified, although with relatively different details with respect to depth, morphology and dimension. However, for a given set of materials and test conditions, the subsurface zones develop towards a quasi-equilibrium state [7]. That is, following an incubation period, observation of subsurface zone characteristics (both composition and morphology) leads to the same results. Expressed in tribological terms, we may speak of a *steady state attrition* that dominates the sliding process unless there are changes in the key variables (contact load, relative sliding speed, etc.) during the test.

In sliding practice, both thermal and mechanical events are interlaced, in the sense that thermal events may change the mechanical properties of the rubbing pair (e.g. hardness yield point, etc.). This change in turn affects the rate of heat release at the surface, thereby altering the thermal and mechanical properties of surface and near surface layers and so on. A useful analogical classification stemming from the thermo-mechanical interdependence within these zones is discussed in reference to *figure 1*, in which the different zones are identified with respect to a steel tribo-specimen that has undergone continuous sliding for some 240 s and reached the quasi-equilibrium wear state for the particular test conditions.

Three distinct zones may be identified.

Zone 1: here the 'compositional mix' is the region closest to the actual sliding interface. The composition of zone 1 is different from the underlying regions in that it consists of the original specimen material, the counterface material, and material from the environment [8]. Thermally, however, zone 1 constitutes a 'thermal skin' that envelops a thin sub-layer from which prospective contact asperities are generated. Severe heating, in the form of strong temperature gradients, is characteristic of this thermal skin: note the severe deformation and orientation of the material grains at the interface.

Zone 2: this zone is characterised by an accumulation of plastic strain, is separated from zone 1 by a compositional interface, and within itself, consists entirely of original specimen material. Temperature rises are augmented by plastic deformation (internal heat generation). The temperature gradients, however, are not as pronounced as those in zone 1: compare the deformation and relative grain orientation in this zone compared to those at the interface. With temperature gradients decaying away from the interface with zone 1, zone 2 represents a transition between the severe temperature rise at the contact interface and the thermally inactive bulk of the material.

Zone 3: this region undergoes elastic strains. In *figure 1*, it follows zone 2. An elastic-plastic interface defines the boundary between these two regions. Like zone 2, region 3 consists entirely of original specimen material. Thermally however, this region may be considered *relatively* inactive.

The dissipation of heat at the interface of dry sliding pairs causes the development of non-uniform temperature gradients in the contacting pair. This restrains the thermal expansion of every volume by the surrounding material, and results in 'temperature-induced distortion', which takes the form of thermal strains, and is directly related to the local temperature gradients in the rubbing pair. This suggests that if the state of thermal strain is characterised, then the temperature distribution in the specimen may be found. Clearly, there are several issues to be considered before implementing this approach. Perhaps of paramount interest is the range and sensitivity of the strain measurements.

1.2. Thermal deformations as temperature indicators

Any temperature-sensitive property or temperature-induced phenomenon of a material can in principal be used to measure temperature. There are many practical considerations which determine the choice of such properties, depending largely upon specific uses. Under all circumstances, however, questions of sensitivity and of range will arise. The thermometric sensitivity depends upon the temperature coefficient of a given property and upon the precision of available methods for measuring small changes of that property.

One direct variation in the state of structure that can be directly related to the temperature is thermal deformation, interpreted in terms of stresses and strains. Thermal strains and stresses set up in any thermal skin determine the thermal distortions of its bounding rubbing surface. Thermal strains may be measured satisfactorily by conventional gauges under moderate temperature gradients. Under high temperature gradients however, most strain gauges become influenced by temperature [9]. So in order to utilise the correlation between the thermal and the mechanical events in tribo-specimens, strains must be evaluated via a measurement technique that is amenable to heat effects. For the most part, this condition is satisfied by non-intrusive strain measurement techniques such as those described in [10–15]. Such methods detect the total displacement components of points within a loaded object, by means of light interferometry (collimated white light or laser). These components are subsequently used to map the mechanical or the thermal strains within the specimen [13–18].

Strain measurements obtained by optical methods can constitute the core of an Inverse Heat Conduction Problem (*IHCP*) [19–21], the goal of which is to determine the temporal frequencies and the flux densities at the interface between the rubbing solids, i.e. in zone 1. The sequence of the solution to this problem is envisaged as entailing two steps. Firstly, thermal strains are obtained for zone 2 (say). The thermal strain

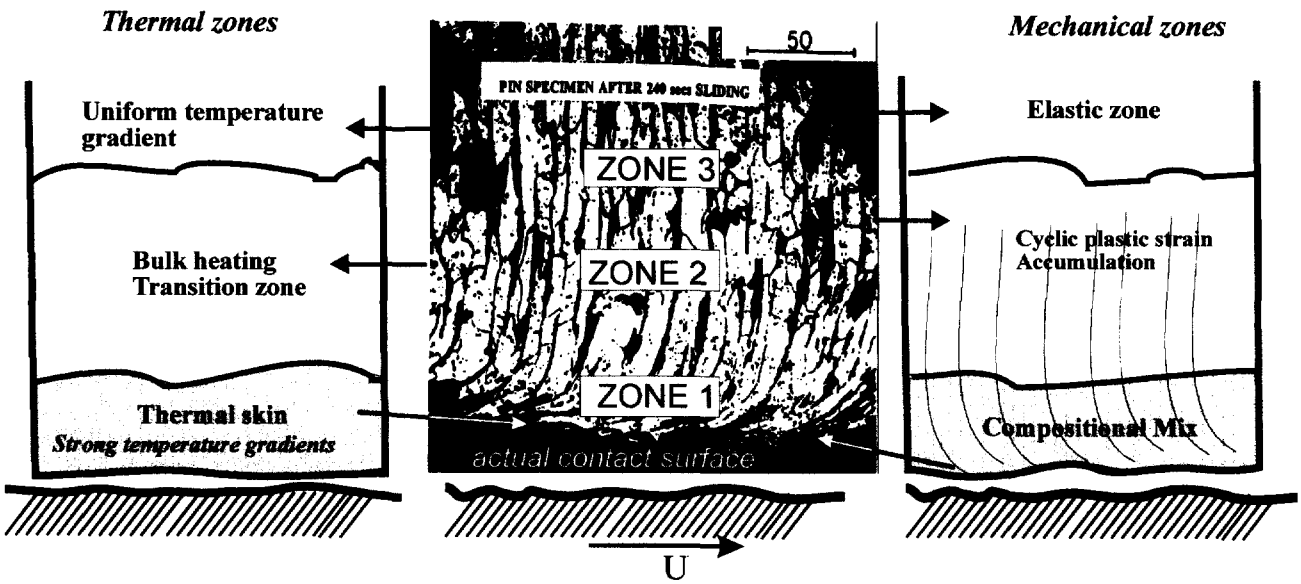

Figure 1. Analogy between the thermal and the mechanical morphological zones developed in sliding tribo-specimens. Note the severity of the traction at the interface, zone 1.

components are then inverted to obtain the local temperature distribution. Secondly, the recovered temperatures are used as remote temperature measurements that may be extrapolated to recover the temperature distribution and the heat flux released at the interface.

This paper deals with the first step of the proposed procedure, namely the teaming together of strain analysis and local thermal expansion to recover the temperature distribution in the cyclic strain zone (zone 2) of a tribo-specimen. The procedure is applied to invert strain data obtained by the analysis of the so-called *double exposure speckle grams* (*DESG*) [18]. Total strain components, obtained for 50 μm surface unit elements, are resolved into elastic, plastic, and thermal components. These in turn are used to construct a system of difference equations, the solution of which completely characterises the strain fields in the said zone. Thermal strains are subsequently fed into a look-up table containing the coefficient of thermal expansion for the particular material at different temperatures to yield an initial temperature distribution. This distribution is refined by iterations to yield an enhanced temperature distribution. The results show satisfactory qualitative agreement with experimental data and with an analytical calibration model.

2. CONCEPT OF LASER SPECKLE PHOTOGRAPHY

Laser-speckle photography techniques have a wide range of scientific and technical applications. The basic concept is well known: when diffusely reflecting objects are illuminated by laser light, there appear to be innumerable infinitesimal point-sources on the object surfaces. As a result, light beams emitted by point-sources interfere with each other in space to form fine, randomly distributed, high-contrast dark or light areas corresponding to destructive or constructive interference, respectively. These areas are called speckles. Speckle size depends on the optical characteristics of the viewing system such as laser wavelength, object size, and image distance. The light intensity distribution of the speckles depends on the propagation of the incident light and the optical diffusivity of the object surface. The light intensity of a given point in space is referred to as the speckle state at that point. If a laser beam is cast on a ground glass plate in the direction of ray 1 as shown in *figure 2*, then the intensity at the viewing point P is determined. When the incident light beam is shifted slightly in angle, say to the direction of ray 2 in *figure 2*, the speckle state at point P changes correspondingly; the speckle state at point P′ is the same as that at point P before the direction of the incident light beam was changed. This phenomenon is called the movement of space speckle, and the distance PP′ is defined as the *speckle displacement*.

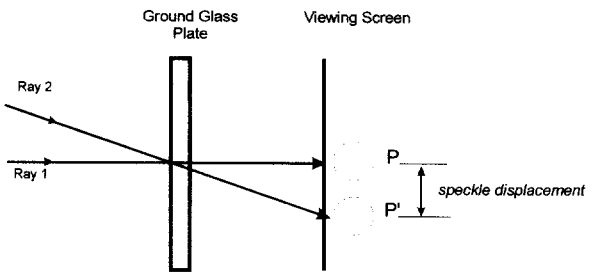

Figure 2. Concept of speckle displacement.

2.1. Double exposure speckle grams (*DESG*)

The technique of DESG exploits the fact that it is possible to expose the same specklegram plate several times, typically once before and once after an 'event' that slightly alters the state of the test object. This DESG permanently *fingerprints* the state of the surface between exposures. Thus for each speckle in one pattern, there is an identical speckle in the second one, shifted as a result of the object deformation. The distances between individual speckle pairs are directly proportional to local in-plane displacements. Moreover, each of the speckle pairs behaves optically in a manner similar to the behaviour of two identical holes separated by a distance when illuminated. Thus, if this speckle pair is illuminated by a coherent light, then fringes similar to Young fringes are formed. So, by recording double exposure photographs of the test object and illuminating the resulting negative so as to generate its optical transform, considerable information about the displacements that have taken place between the exposures can be gained.

Figure 3 [9] shows the main features of the system utilised in the current work to record DESGs. A pulsed ruby laser beam is used to illuminate the

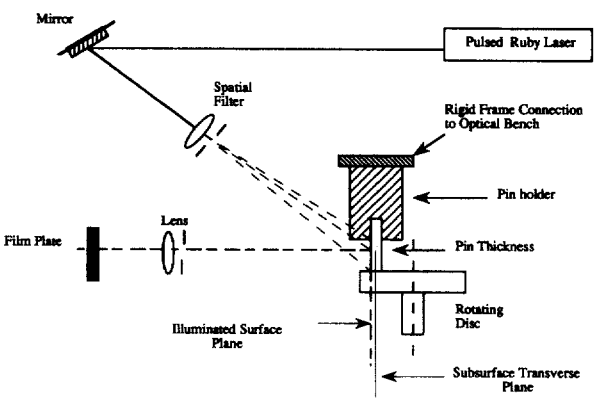

Figure 3. Basic features of the system used to record DESG.

transverse plane of a stationary pin specimen in sliding contact against a rotating counterface disk. In order to obtain speckle displacements the specklegram must be reconstructed. There are two methods for reconstructing a speckle-gram: point-by-point analysis and full-field view. Since the first method was applied in the current work, a summary of its basic features is given below.

2.2. Point-by-point analysis of DESG

Figure 4a illustrates an optical reconstruction system for point-by-point analysis. Other aspects of the optical system used both to record and interpret speckle-grams can be found elsewhere [10–12]. Re-illuminated by an unexpanded narrow laser beam (*figure 4b*), each portion of the specklegram reveals a diffraction pattern (consisting of a bright central spot and a diffraction halo of lesser light intensity) and a series of equally spaced Young fringes on the viewing screen. The orientation of the fringes at a point is unique to the amount of deformation at this particular point. The relation

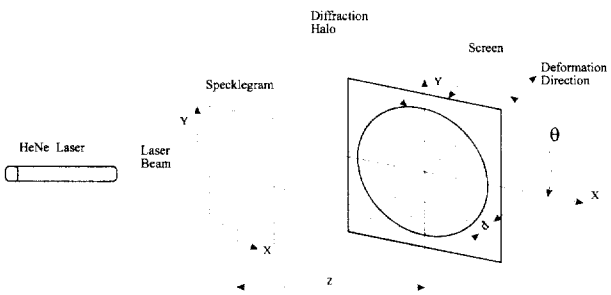

a

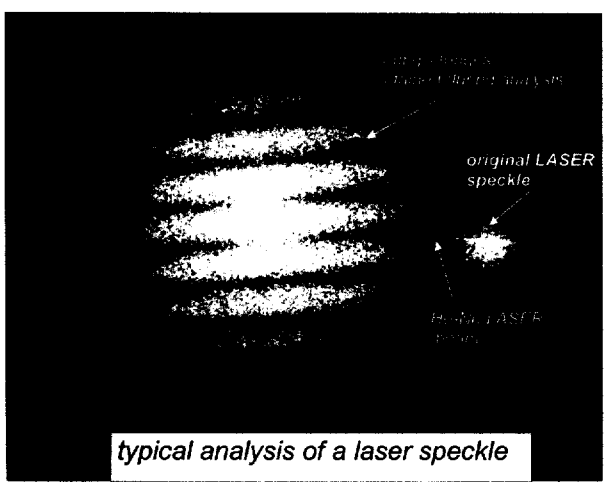

b

Figure 4. Analysis of DESG. **a**: diagram of the optical system applied in a point-by-point analysis of specklegrams; **b**: typical point-by-point analysis of a specklegram.

between the fringe spacing and the speckle displacement satisfies the well-known Young interference formula:

$$U = \frac{\lambda Z}{M d} \tag{1}$$

The direction of the speckle displacement is normal to the Young fringes. The horizontal and vertical displacement components are determined from the relations:

$$u = U \cos\theta \tag{2}$$

$$v = U \sin\theta \tag{3}$$

where θ is the angle between the displacement vector U and the X-axis. Once the displacement components are found from *DESG* analysis, it is possible to reconstruct the *total equivalent strain fields* in the horizontal X- and the vertical Y- directions by applying a discretised version of the Lagrangian description of the strain (see appendix). In this manner, a full description of the total strain components in the X- and Y- directions is obtained.

3. DESCRIPTION OF THE METHOD

It is common to resort to numerical techniques to resolve the strain fields in a given specimen. The numerical methodology is well-known: by dividing the domain of interest into infinitesimal elements, algebraic alternatives to the differential or integral forms of the governing equations may be constructed for each unit element. By so doing, the strain fields are represented by a system of algebraic simultaneous equations, the solution of which maps the strain fields in the specimen. This idea is employed here to construct a system of equations, based on the optically measured displacement vectors, that represents the various strain contributions (elastic, plastic and thermal) for each of infinitesimal surface elements. When the displacements are processed in the so-called *point-by-point* mode, the equivalent *total strains* are obtained with significant resolution. However, to completely characterise the strain fields, optical measurements must be complemented by a procedure which extracts from the total strains the information concerning the individual strain contributions-elastic, plastic and thermal.

3.1. Strain characterisation

The total strain of any elasto-plastic element is a superposition of three strain components: elastic, plastic, and thermal. Hence the strain components in the X- and the Y- directions may be expressed as:

$$\varepsilon_x^{\mathrm{T}} = \varepsilon_x^{\mathrm{e}} + \varepsilon_x^{\mathrm{p}} + \varepsilon_x^{\mathrm{th}} \tag{4}$$

$$\varepsilon_y^{\mathrm{T}} = \varepsilon_y^{\mathrm{T}} + \varepsilon_y^{\mathrm{p}} + \varepsilon_y^{\mathrm{th}} \tag{5}$$

The strain distribution near the contact surface may be used to compute an equivalent (or an effective) strain distribution that is a function of the depth from the surface. Consider a unit element subject to uniaxial loading and shear deformation under plane stress conditions. For such an element, the equivalent total strain $\mathrm{d}\bar{\varepsilon}$ is defined as:

$$\mathrm{d}\bar{\varepsilon} = \frac{2}{3}\left[\frac{1}{2}\left[(\mathrm{d}\varepsilon_x - \mathrm{d}\varepsilon_y)^2 + (\mathrm{d}\varepsilon_z - \mathrm{d}\varepsilon_y)^2 + (\mathrm{d}\varepsilon_x - \mathrm{d}\varepsilon_z)^2\right] + 3\,\mathrm{d}\varepsilon_{xy}^2\right]^{\frac{1}{2}} \quad (6)$$

The information needed to calculate the total equivalent strain is readily available from optical measurements, except for the strain in the Z-direction ε_z. This may be assumed *initially* to equal the strain in the X-direction. Once the equivalent total strain has been computed, the equivalent plastic strains can be determined from:

$$\bar{\varepsilon} = \varepsilon_{\mathrm{ep}}^x + \frac{2\,(1+\mu)}{E}\,\sigma_{\mathrm{e}}^x \quad (7)$$

$$\bar{\varepsilon} = \varepsilon_{\mathrm{ep}}^y + \frac{2\,(1+\mu)}{E}\,\sigma_{\mathrm{e}}^y \quad (8)$$

where σ_{e}^x and σ_{e}^y are the equivalent stresses corresponding to the total-strain states ε_x and ε_y respectively. The relation between the equivalent stresses and the total strains is contained in the uniaxial stress-strain curve. Hence for any selected value of the total strain, the value of the equivalent stress can be determined either graphically or by providing a computerised look-up-table. Once the equivalent total strain and the equivalent plastic stress components σ_{ep}^x and σ_{ep}^y are determined. The components of the plastic strain are determined from:

$$\varepsilon_x^{\mathrm{p}} = \frac{\varepsilon_{\mathrm{ep}}^x(2\,\varepsilon_x^{\mathrm{T}} - \varepsilon_y^{\mathrm{T}} - \varepsilon_z^{\mathrm{T}})}{3\,\bar{\varepsilon}} \quad (9)$$

with cyclic relations for the other strain components. The fact that the analysis is mainly confined to the cyclic plastic strain zone, zone 2, may be employed to augment the strain analysis by exploiting the constant volume characteristics of plastic deformation: for the part of the material experiencing plastic deformation, no change in volume takes place. Expressed in terms of plastic strain, this condition can be written as:

$$\varepsilon_x^{\mathrm{p}} + \varepsilon_y^{\mathrm{p}} + \varepsilon_z^{\mathrm{p}} = 0 \quad (10)$$

Now if the specimen undergoes uniaxial loading, then the relation between the plastic strain components assumes the form:

$$\varepsilon_x^{\mathrm{p}} = \varepsilon_z^{\mathrm{p}} = -\frac{1}{2}\,\varepsilon_y^{\mathrm{p}} \quad (11)$$

Equations (9), (10) and (11) constitute a system of three equations in three unknowns ($\varepsilon_x^{\mathrm{p}}$, $\varepsilon_z^{\mathrm{p}}$, and $\varepsilon_z^{\mathrm{p}}$), the solution of which yields a preliminary estimate of the in-plane plastic strain component and an enhanced estimate of the out-of-plane equivalent strain component $\varepsilon_z^{\mathrm{T}}$. This estimate may be subsequently refined through consecutive iterations until the solution converges to a prescribed degree of accuracy.

3.2. Strain–temperature analysis

The general expression for the thermal strain in a unit element of a material may be expressed in terms of the thermal expansion as:

$$[\varepsilon_x^{\mathrm{th}}]_{ij} = [\alpha(T)\Delta\,T]\,\delta_{ij} \quad (12)$$

In general, the coefficient of thermal expansion is a symmetric tensor. However, for materials of a cubic lattice structure, such as steels, this coefficient is equal in all directions [22], i.e. $\alpha_{ij} = \alpha_{ji} = \alpha$. So the thermal strains can be written as:

$$\varepsilon_x^{\mathrm{th}} = \alpha(T)\,\Delta T x \quad (13)$$

$$\varepsilon_y^{\mathrm{th}} = \alpha(T)\,\Delta T y \quad (14)$$

It follows that once the thermal strain components are known, equations (13) and (14) may be used to deduce the temperature rise in a particular unit element. This process is performed in two steps. Firstly, the α–T curve of the material is plotted as an α–αT curve. Then the directional components of the thermal strain are fed into this new curve and a provisional temperature T' is obtained. Secondly, the provisional temperature is fed into the original α–T curve and the respective value of the coefficient of thermal expansion is substituted in equation (13) or (14) to deduce an enhanced estimate of the temperature rise. The process may be repeated to refine the temperature estimates until the solution converges. The procedure is illustrated graphically in *figure 5*. The plots in the figure represent typical thermal strain–temperature and coefficient of thermal expansion–temperature plots for mild steel *AISI 1020*.

4. APPLICATION TO AVAILABLE DATA

In this section, the results of applying the proposed procedure to invert the strains measured in the cyclic plastic zone, zone 2, of a thin metallic pin-specimen is presented. The rectangular cross-sectioned pin slides against a counter-face rotating disk (*figure 6*). Strain data were obtained during sliding in-situ for several points on the pin. The relative locations of these points on the specimen are illustrated in *figure 7*. Conditions of sliding and dimensions of the specimens are summarised in the *table*. As described elsewhere [18, 19], local deformation vectors were obtained by the analysis of (*DESG*). The pin-specimen was modelled

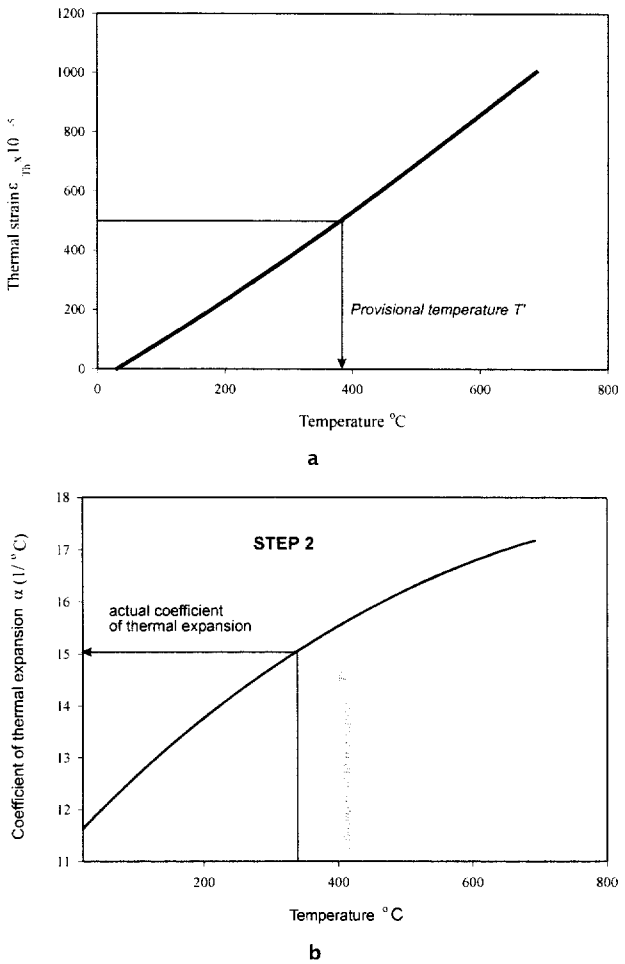

Figure 5. Schematic illustration of the procedure for the extraction of temperatures from thermal strain data. Step 1: extraction of a provisional temperature T'; step 2: extraction of the enhanced coefficient of thermal expansion.

as a rectangular cantilevered beam subject to uniaxial compression and a shearing friction force as depicted schematically in *figure 8*.

Figure 9 is a plot of the *measured* finite total strains ε_x^T and ε_y^T, along the specimen's vertical centreline [18] after 240 seconds of sliding. The points, along the vertical centreline of the pin, for which the strains are plotted, are shown in *figure 10*. The measured strains were found to be consistent with the optically determined directional displacements and with the subsurface metallographic examinations. Interestingly, it was found that despite the large displacements in the X-direction, as compared to those in the Y-direction, the horizontal strain components were relatively smaller than the vertical strains, indicating a thermal strain higher in the X-direction than in the Y-direction.

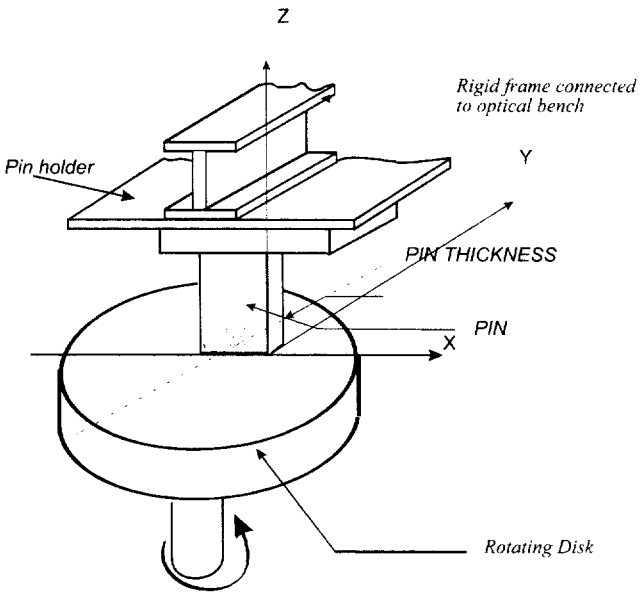

Figure 6. Diagram of the pin-disk arrangement.

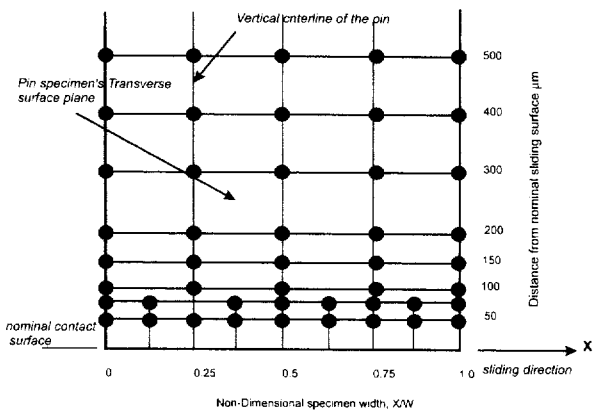

Figure 7. Arrangement of the points on the pin used for strain inversion.

TABLE Summary of sample dimensions and sliding conditions.	
Pin material	mild steel *AISI 1020*
Disk material	carbon steel *AISI 1018*
Nominal normal load (N)	80
Specimen dimension	6 mm × 1 mm
Sliding speed ($m \cdot s^{-1}$)	0.5
Nominal stress (MPa)	13.33
Nominal coefficient of friction	0.57

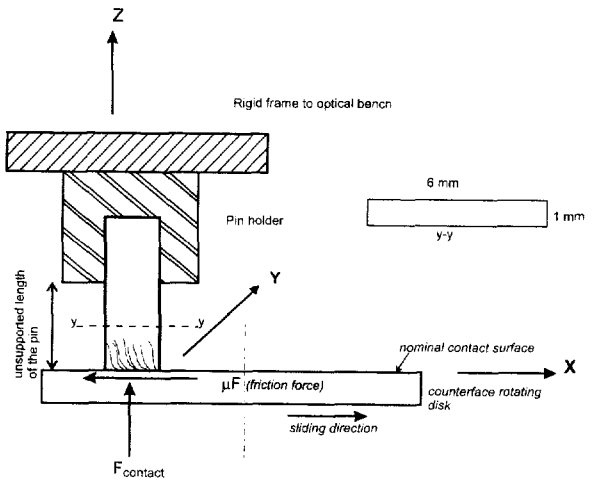

Figure 8. Diagram of the forces acting on the pin specimen.

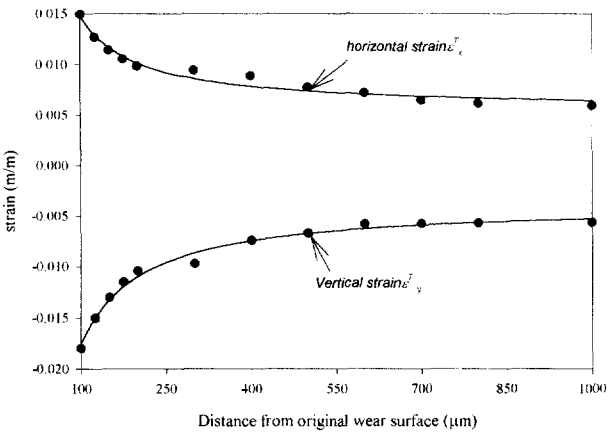

Figure 9. Variation of the measured strain components along the specimen's vertical centreline.

Figure 11 depicts the extracted horizontal and vertical thermal strains $\varepsilon_x^{\text{th}}$ and $\varepsilon_y^{\text{th}}$. The components of the thermal strain were computed by means of the procedure detailed above. Note that the deduced thermal strains are consistent with the measured total strains. That is to say, the horizontal thermal strains are relatively higher than the vertical thermal strains. By contrast the gradients of the latter (especially at the vicinity of the nominal contact surface) are stronger than those of the former. This may be explained in view of the resistance to the free expansion of the material. The resistance offered by the contacting (compressive) forces in the vertical Y-direction would tend to restrict the vertical thermal expansion of the material. In the horizontal X-direction however, the material is relatively free to expand. For this reason, the material will experience higher thermal strains in the X-direction than those experienced in the Y-direction. Away from the nominal contact surface, both

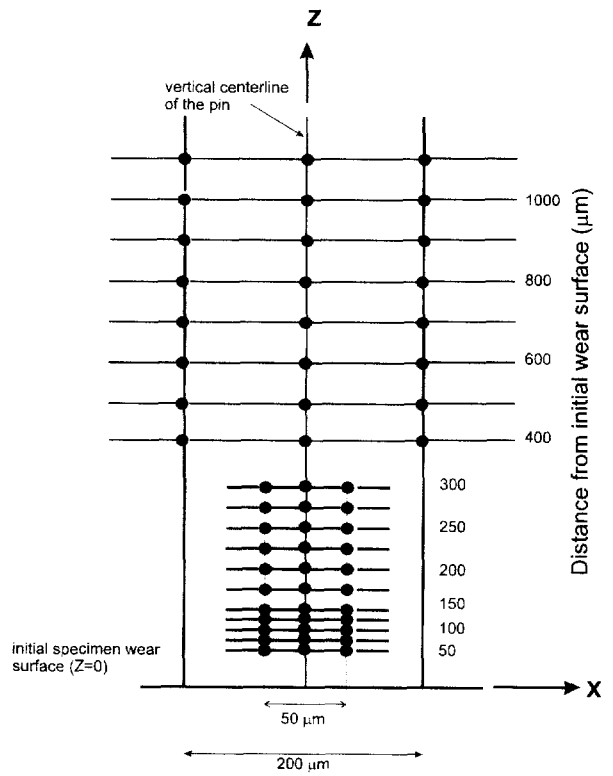

Figure 10. Diagram of the points on the vertical centreline of the pin for which the temperature distribution is plotted.

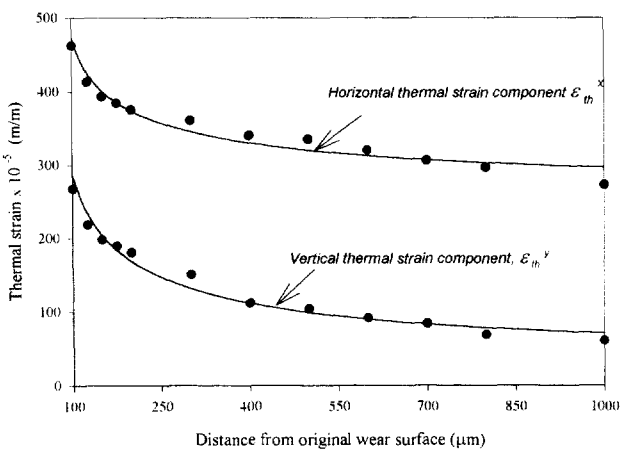

Figure 11. Variation of the vertical and the horizontal thermal strain components along the specimen's vertical centreline.

the influence of temperature gradients and the influence of the contact forces are weaker than the corresponding influence at the surface. This frees the material to expand relatively unobstructed in both directions, in proportion to the local temperature gradients. This is

the explanation why the uniformly decaying thermal strain gradients are displayed away from the surface (some 400 μm from the surface).

Figure 12 is a plot of the horizontal and vertical temperature rises along the specimen's vertical centreline. Conditions are the same as those of *figures 9* and *11*. Two plots are presented in the figure. Solid symbols represent the temperatures as deduced from the strain inversion process. The second plot (solid line) represents the best fit to the extracted temperatures. As expected, the temperature rise closer to the nominal contact surface is higher than that experienced away from that surface. Moreover, the gradients in both directions are of comparable, moderate, magnitude. On the other hand, the horizontal temperature rise is higher than the vertical rise. This may be attributed to heat diffusion effects: as the pin slides, heat will diffuse in a direction opposite to the direction of motion. The diffusion in the X-direction, however, will dominate over the diffusion in the Y-direction [23]. Consequently, the local temperature gradients will be inversely proportional to the position with respect to the leading edge of the pin-specimen. The farther from the leading edge a given point is, the higher the horizontal temperature gradient Δ^{T}_{xx}.

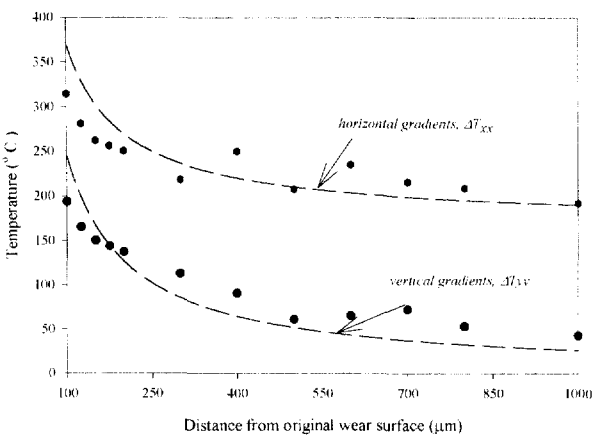

Figure 12. Development of the horizontal and the vertical temperature gradients along the specimen's vertical centreline.

The temperatures plotted in *figure 12* agree qualitatively with the results reported by other researchers for the sliding of steel on different materials. A direct comparison however cannot be established since in general the conditions of the reported experiments differ from the current one. In any event however, both experimental [24] and analytical modelling [25] indicate temperatures in excess of 700 °C for the sliding of steel *Fe360A* over *Retinax* and above 1 000 °C (at about 1 mm from the contact surface) for steel *AISI 52100* rubbing against a disc of the same material [26]. This agrees fairly closely with the current estimates, given the difference in the experimental conditions.

5. COMPARISON WITH A THEORETICAL MODEL

To calibrate the results of the proposed strain-inversion procedure, an analytical model of the pin specimen was developed, based on the Duhammel theorem.

The temperature field in the surface layer during sliding friction is, strictly speaking, a three-dimensional heat transfer problem. In order to simplify the analysis, without loss of generality, the three-dimensional heat flow fields may be replaced by a one-dimensional model yielding average temperatures at different layers of the solid, provided that it is understood that these temperatures are mere indicators of the general trend of the temperature profile in the solid and not strictly accurate estimates.

The equation of heat conduction under conditions of sliding and wear may be written as:

$$\frac{\partial T(x,t)}{\partial t} = a\,\frac{\partial^2 T(x,t)}{\partial x^2} \tag{15}$$

Initial and boundary conditions may be written as:

$$T(0,t) = f_1(t) \tag{16}$$

$$T(L,t) = f_2(t) \tag{17}$$

$$T(x,0) = 0 \tag{18}$$

where a is the thermal diffusivity, x is the variable distance and L is a selected constant distance. Equations (15-18) may be transformed into:

$$\frac{\partial \psi(z,t,T)}{\partial t} = a\,\frac{\partial^2 \psi(z,t,T)}{\partial z^2} \tag{19}$$

and

$$\psi(0,t,T) = f_1(T) \tag{20}$$

$$\psi(0,t,T) = f_2(T) \tag{21}$$

$$\psi(z,0,T) = 0 \tag{22}$$

The solution of the system (19-22) may be derived by means of the Duhammel theorem as in [26]:

$$\psi(z,L,T) = f_1(T)\left[1 - \frac{z}{L} - \frac{2}{L}\sum_{m-1}^{\infty} \exp\{-a\beta_m^2 t\}\frac{1}{\beta_m}\sin\beta_m z\right] + f_2(T)\left[\frac{z}{L} + \frac{2}{L}\sum_{m-1}^{\infty} \exp\{-a\beta_m^2 t\}\frac{1}{\beta_m}\sin\beta_m z\cos m\pi\right] \tag{23}$$

where:

$$\beta_m = \frac{m\pi}{L} \qquad (m = 1,2,3\ldots)$$

Therefore:

$$\psi(z,t-T,T) = f_1(T)\left[1 - \frac{z}{L} - \frac{2}{L}\sum_{m=1}^{\infty}\exp\{-a\,\beta_m^2(t-T)\}\frac{1}{\beta_m}\sin\beta_m z\right] + f_2(T)\left[\frac{z}{L} + \frac{2}{L}\sum_{m=1}^{\infty}\exp\{-a\,\beta_m^2(t-T)\}\frac{(-1)^m}{\beta_m}\sin\beta_m z\right] \tag{24}$$

so that [26]:

$$T(z,t) = \frac{\partial}{\partial t}\int_0^t \psi(z,t-T,T)\,\mathrm{d}T \tag{25}$$

Substituting from equation (24) by the function $R(z,t-J,J)$ into equation (27) and performing the integral, the temperature at any location may be written as:

$$T(z,t) = \frac{\partial}{\partial t}\left[f_1(T)\left(1 - \frac{z}{L} - \frac{2}{L}\sum_{m=1}^{\infty}\exp\{-a\,\beta_m^2(t-T)\}\frac{1}{\beta_m^3}\sin\beta_m z\right) + f_2(T)\left(\frac{z}{L} + \frac{2}{L}\sum_{m=1}^{\infty}\exp\{-a\,\beta_m^2(t-T)\}\frac{(-1)^m}{\beta_m^3}\sin\beta_m z\right)\right]_0^t \tag{26}$$

On substituting the limits in equation (26) and differentiating with respect to the time parameter t, the expression for the temperature assumes the form:

$$T(z,t) = f_1(t)\left[1 - \frac{z}{L}\right] - \frac{2}{L}f_1(t)\sum_{m=1}^{\infty}\exp\{-a\,\beta_m^2\,t\}\frac{1}{\beta_m}\sin\beta_m z + f_2(t)\left[\frac{z}{L}\right] + \frac{2}{L}f_2(t)\sum_{m=1}^{\infty}\exp\{-a\,\beta_m^2\,t\}\frac{(-1)^m}{\beta_m}\sin\beta_m z \tag{27}$$

Recalling the definition of β_m and noting that the term $\exp\{-a\,\beta_m^2\,t$ decays rapidly, it will be noticed that beyond the first term, i.e. at $m = 1$, all the following terms in the exponential series of equation (27) are practically zero. This also may be verified through a straight forward scaling argument in which (using $a \propto 10^{-5}$ m^2·s^{-1} and $L \propto 10^{-6}$ m) it should be realised that only the first term β_1 has a significant value, whereas the following terms are of the order $\exp\{-10^{19}\,\pi\}$, which is practically zero. So the temperature at any location would be fairly represented by the expression:

$$T(z,t) \approx \left[1 - \frac{z}{L}\right]f_1(t) + \frac{z}{L}f_2(t) - \frac{2}{\pi}[f_1(t) + f_2(t)]\exp\left\{-a\,\frac{\pi^2}{L^2}\,t\right\}\sin\left(\frac{\pi}{L}\right)z \tag{28}$$

In order to apply equation (28) to the experimental conditions at hand, the functions $f_1(t)$ and $f_2(t)$ have to be evaluated.

The function $f_2(t)$ represents the temperature rise at the far end of the affected portion of the pin. This may be interpreted in either of two ways. On the one hand, we may consider that $f_2(t)$ represents the temperature rise at the bulk of the material. This so-called bulk temperature rise may be calculated by means of some of the published models such as that of Lim and Ashby [28] (see appendix). Alternatively and in contrast, the function $f_2(t)$ may be taken to represent the temperature rise at the end of zone 3, where the temperature rise above the ambient temperature is practically zero. In both interpretations however, the location of the temperature, represented by the function $f_2(t)$, with respect to the original wear surface, has to be evaluated. This may be accomplished by means of metallographic inspection or, alternatively, by means of DESG analysis.

If the first convention is adopted, then $f_2(t)$ will indicate a bulk temperature rise which is significantly less than the flash temperature rise encountered at the actual frictional interface, surface $Z = 0$ in *figure 1*. A direct consequence of this interpretation is that the bulk temperature rise occurs approximately at the interface of zones 2 and 3 in *figure 1*. That is, it occurs, in mechanical terms, at the elastic-plastic interface, where it is assumed that the extension of that interface away from the actual contact surface is time-dependent prior to the establishment of the steady state wear rate (see section 1). While the location of the interface Z_{2-3} may be determined by metallographic examinations (where plastically deformed material grains cease to exist), a practical indicator for the location of that interface may be deduced from DESG analysis: the oscillation of the strain components for different neighbouring locations around a common value. For example if at several neighbouring Z-planes (Z_a, Z_b, and Z_c, say), the strain components are found to be:

$$\varepsilon_{x_z} = \Delta_x \pm \delta^x_{\mathrm{a,b,c}} \qquad \delta <<< \Delta \tag{29}$$

and

$$\varepsilon_{y_z} = \Delta_y \pm \delta^y_{\mathrm{a,b,c}} \qquad \delta <<< \Delta \tag{30}$$

then it may be assumed that the bulk temperature rise occurs at the location where that oscillation takes place. In our experience, this criterion is fairly accurate as compared with other optical and metallographic procedures.

If the second convention for the function $f_2(t)$ is adopted however, the practical value of that function would be zero. In this case, the location of that plane where $f_2(t)$ is zero must be found strictly from DESG analysis, and it is represented by the locations where no elastic or plastic strain components are encountered. Again, it is implied that the extension of that surface where no strains are present relative to the original wear surface is relatively time-dependent until steady state wear is established.

The function $f_1(t)$ meanwhile represents the average temperature at the interface between zones 1 and 2. This surface would be strongly affected by the temperature pulses originating at the frictional interface and penetrating through the micro-roughness towards the bulk of the material (zones 2 and 3). If a reasonable, *average*, estimate of the strength of a temperature pulse at the interface is readily available (such as that of reference [28]), then this estimate may be related to the function $f_1(t)$. This may be achieved by assuming that in order for its effect to be felt, an interfacial temperature pulse has to penetrate through zone 1 before it affects the boundary at zone 2. So if the location at which this pulse loses its strength is determined, then an interpolation, based on the thickness of zone 1, may be performed to determine the relative strength of the pulse when it reaches the interface Z_{2-3}. In this case, the strength of the pulse at this plane represents the value of the function $f_1(t)$. Again, it is important to note that the thickness of zone 1, which is essential to any estimate of $f_1(t)$, may be found by means of metallographic inspection.

Admittedly however, the evaluation of $f_1(t)$ introduces some uncertainty stemming from the nature of the assumptions implied in the process. These may be summarised as follows: (1) the flow of heat in zone 1 is assumed to be one-dimensional; (2) the strength of the pulse is constant, and (3) the maximum penetration depth of the pulse is calculated from the linearised one-dimensional solution of the heat equation. The effects of these assumptions on the model are discussed within the context of developing the model equations used to determine the strength of the pulse at the interface Z_{2-3}.

5.1. The penetration depth of a temperature pulse

Consider the semi-infinite plane shown in *figure 13*. The material and its surface are at some given initial temperature θ_0. At the time t_0^+, the surface is set to a temperature $\theta_s(t)$, where $t \leq t_c$. Now define a normalised temperature θ^- representing the ratio of the temperature rise at a depth Z to the surface temperature. One obtains:

$$\overline{\theta}(t) = \frac{\theta_z(t)}{\theta_s(t)} \tag{31}$$

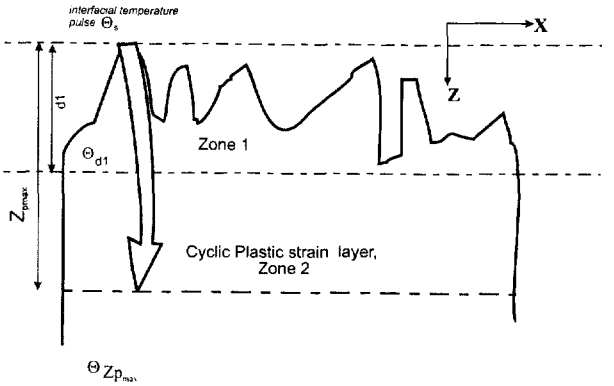

Figure 13. Penetration depth of a temperature pulse.

The temperature field in the material of the layer may be given by:

$$\frac{\partial \overline{\theta}}{\partial t} = a \frac{\partial^2 \overline{\theta}}{\partial Z^2} \tag{32}$$

with the boundary conditions:

$$\begin{aligned} \overline{\theta} &= 0 \qquad t < 0, \quad 0 < z < \infty \\ \overline{\theta} &= 1 \qquad t > 0, \quad z = 0 \end{aligned} \tag{33}$$

The solution to this problem is:

$$\overline{\theta} = \frac{2}{\sqrt{\pi}} \int_{\xi}^{\infty} \exp\{-\xi^2\}\, \mathrm{d}\xi = \mathrm{erfc}(\xi) \tag{34}$$

where:

$$\xi = \frac{Z}{2\sqrt{at}} \tag{35}$$

The solution, equation (34), may be regarded as the response of the material to a surface temperature pulse. So the maximum response corresponds to $\theta = 1$, whilst no response is $\theta^- = 0$, i.e. $0 < \theta_p < 1$.

The equation:

$$\overline{\theta}_p = \frac{2}{\sqrt{\pi}} \int_{\xi_p}^{\infty} \exp\{-\xi^2\}\, \mathrm{d}\xi = \mathrm{erfc}(\xi_p) \tag{36}$$

has the solution (ξ_p), unique to a particular θ_p, such that:

$$Z_p = 2\,\xi_p \sqrt{a\,t} \tag{37}$$

is defined as the penetration depth of θ_p. It follows that a unit temperature pulse on the surface causes a temperature rise of at least θ_p to penetrate to a depth Z_p. As an example (using $\mathrm{erfc}(0.275) = 0.7$), $\theta_p = 0.7$ (a rise of at least 70 percent of the original pulse) is felt at a depth of:

$$Z_{0.7} = 0.275 \times 2\sqrt{at} \tag{38}$$

If the maximum penetration depth is defined as the depth at which a temperature rise of about 1 percent of the temperature rise at the surface is located, i.e. $Z_{0.01}$, then this depth is given by (after using erfc(2) $\approx$ 0.01):

$$Z_{\mathrm{Pmax}} = Z_{0.01} \cong 4\sqrt{a\,t} \tag{39}$$

Now, if the thickness of zone 1 is determined to be d_1, then it is necessary to calculate the relative strength of the pulse at the interface between zones 1 and 2. This is determined as follows:

a) the ratio of the distance travelled by the pulse to the maximum penetration depth is found from:

$$\xi_{d_i} = \frac{d_1}{4\sqrt{a\,t}} \tag{40}$$

b) the relative strength of the pulse is determined from:

$$\overline{\theta}_{d_1} = \mathrm{erfc}(\xi_{d_1}) \tag{41}$$

c) finally the value of the function $f_1(t)$ is calculated from:

$$f_1(t) = \overline{\theta}_{d_1}\, T_{\mathrm{fl}} \tag{42}$$

where T_{fl} is the flash temperature.

Note that this model is one-dimensional. So in this situation, the temperatures calculated by means of equation (28) represent an average temperature of a subsurface layer at a distance Z from the original wear surface. The maximum penetration depth (equation (39)) is calculated under the assumption that the diffusivity of the material remains unaffected by the heat release and by plastic deformation. This might introduce a slight error in the value of $f_1(t)$. The accuracy of that estimate might be enhanced by treating the specimen as a composite region of different diffusivities. However this approach would involve trial solutions that must be iterated since the temperature distribution is not readily available. So the level of accuracy gained may not be worth the computational effort.

Figure (14) depicts a comparison between the vertical temperature gradients ΔT_{yy} obtained by the proposed strain inversion technique, and those computed from equation (28). In evaluating equation (28), the function $f_2(t)$ was assumed to represent the bulk temperature rise. The location of that temperature was assumed to be located at the interface between zones 2 and 3, i.e. at an estimated distance of 600 µm from the nominal wear surface (as verified by metallographic examination). The magnitude of the bulk temperature was calculated from equation (14) of reference [28]. The function $f_1(t)$ was calculated by applying the interpolation technique described above. Thus, the thickness of zone 1 was estimated metallographically to be around 100 µm from the nominal contact surface. The flash temperature was computed from equation (8) of reference [28], and the maximum penetration depth was calculated by means of equation [40].

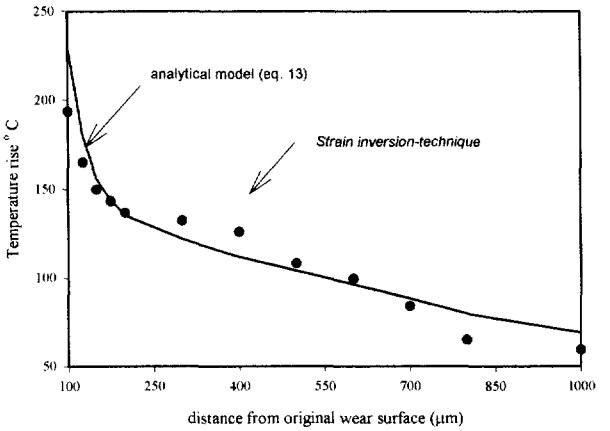

Figure 14. Comparison between the vertical temperature gradients (resulting from strain inversion) with the analytical model (equation (13)).

It will be noticed that the temperatures obtained by both methods are in excellent agreement closer to the interface with zone 1 (about 100 µm–300 µm) away from the wear surface). This agreement is relatively close starting some 400 µm from the surface. This may be an effect of the distance between the points examined – about 25 µm in the first region and approximately 100 µm to 200 µm for the second region (refer to *figures 7* and *10*). This results in a greater number of points examined closer to the interface than analysed beyond the 300 µm marker, thus allowing a more accurate reflection of the state of heating closer to the interface than that in the following sub-layers. This may suggest a maximum critical distance (and thereby a minimum number of points analysed in a given layer of the solid) that must be maintained between the analysed points so as to satisfy a preset level of resolution. Admittedly, an investigation of the effect of the distance between the analysed points on the accuracy of the recovered temperatures was not performed due to the absence of larger data sets. But in any case, the overall agreement between the analytical model and the recovered temperatures is satisfactory given the average nature of the model.

5.2. Remarks on the accuracy of the method

The proposed strain inversion technique poses some intriguing questions pertaining to the accuracy of the estimated temperatures. Like other methods, the current technique might encompass some errors. These do not stem from the underlying concept, but originate from the nature of the parameters comprised in the procedure. The parameters involved may be classified as:

a) parameters pertaining to the strain measurement technique, such as the accuracy of the optical system

used in the recording and the analysis of DESG, the number of points on the specimen which are used to reconstruct the strain fields, and the frequency of exposures;

b) parameters that are related to the mechanics of the specimen, such as the state of loading and the extension of the plastic zone (zone 2);

c) parameters pertaining to the physical properties of the material such as the accuracy of the thermal expansion data, and the nature of the thermal expansion of the material (isotropic or anisotropic).

The number of points used to reconstruct the strain fields impacts on the accuracy of the total strain components. A high number of points implies a smaller spacing between the points analysed so that the effect of the non-linearity of the strain between points is minimised. To visualise the effect of the number of points analysed, one may draw an analogy with the effect of the number of nodal points on the accuracy of a numerical solution in finite-difference schemes. The minimisation of the intervals between nodal points in a computational domain has a direct effect on the accuracy of any numerical solution of a partial differential equation, for example. This effect may be displayed in the form of the stability of a solution, i.e., suppressing the error introduced through the discretisation of a continuum.

In general, an increase in the frequency of exposures is broadly expected to have an effect similar to that of increasing the number of points on the accuracy of the reconstructed total strains. It is natural to expect that increasing both the number of analysed points and the frequency of DESG should effectively enhance the accuracy of the total strains and thereby the accuracy of the inverted temperatures, and should in a sense accelerate the convergence of the method. It follows that an optimal combination of number of points and number of exposures ensuring maximum accuracy of the total strains may exist.

A pivotal parameter that affects the procedure is the state of loading of the specimen: if the specimen undergoes a simple combination of loading, such as that encountered in the present case, the expression of the governing stress-strain equations in discretised form may be relatively straightforward. For complicated load combinations however, this may not be so simple. Nevertheless, in principal, a discretised alternative can be devised. In such case, components may not be related in a straightforward manner.

The state of voids or impurities within the test specimens is closely related to how closely the published data of a certain property, such as thermal expansion, truly represent the properties of the particular specimen. Of course, for a void-free specimen the inversion part of the technique should be highly accurate and vice-versa. Testing more 'identical' specimens under identical conditions would enhance the results. In any event, the effect of the impurities on the accuracy of the inverted temperatures is less pronounced compared to the effect of the other factors mentioned above.

Finally, the accuracy of the method can be enhanced by compensating for the variation in the thermal conductivity with temperature. Note that the inverted temperatures are in effect a solution to the heat equation. In the current work the constant conductivity solution of the heat equation was obtained by strain inversion. This may be enhanced by observing that the resulting temperatures are a solution of a transformed quasi-linearised heat equation. A back transformation that includes the conductivity-temperature relation of the material may be then applied to obtain the enhanced variable conductivity solution (see for example Abdel-Aal and Smith [29]). However a note of caution is due, since the nature of the conductivity- temperature relation for the material may not lend itself to an easy back transformation that is directly applicable to the data.

6. SUMMARY AND CONCLUSIONS

A procedure to utilise thermal strains developed in tribo-specimens as temperature indicators has been presented. The procedure involves two steps. The first characterises the thermal strain fields in a region close to the actual rubbing surface. These in turn are inverted to yield a temperature distribution in that zone. The second step entails the inversion (extrapolation) of these remote temperatures to recover the temporal frequencies and the flux densities at the rubbing interface.

The current work treated the first step in this procedure through the analysis of optically measured strains in thin steel pin-specimens in sliding contact. The results were compared with some published data, and overall agreement between the estimates of the current method and the published data was satisfactory.

The procedure is facilitated through teaming the analysis procedure together with non- intrusive strain measurement techniques (e.g. optical methods). This may be utilised to characterise thermally species operating within hostile tribological environments.

Acknowledgement

Part of this work was sponsored by the Army Research Office, Engineering Science Division, under grant no: DAAL-03-91-G-0246 (scientific officer: Dr. K. Iyer). The author is indebted to Dr. M.A. Seif of Tuskegee University AL, USA, and Dr. R. Keanini of UNCC for many valuable discussions and interesting comments.

REFERENCES

[1] Czichos H., Tribology. A System's Approach to the Science and Technology of Friction Lubrication and Wear, Elsevier, Amsterdam, 1978.

[2] Blok H., Measurement of temperature flashes on gear teeth under extreme-pressure conditions, in: General discussion on lubrication and lubricants, Proc. Inst. Mech. Eng. London 2 (1937) 14–23.

[3] Blok H., Theoretical study of temperature rise at surfaces of actual contact under oiliness lubricating conditions, in: General Discussion on Lubrication, Proc. Inst. Mech. Eng. London 2 (1937) 222–235.

[4] Blok H., The postulate about the constancy of scoring temperature, NASA sp-237, Washington DC, 1970.

[5] Jaeger J.C., Moving sources of heat and temperatures at sliding contacts, Proc. Roy. Soc. NSW 56 (1942) 203–222.

[6] Archard J.F., The temperature of rubbing surfaces, Wear 2 (1958) 438–455.

[7] Rice S.L., Nowtony H., Wayne S.F., Characteristics of metallic subsurface zones in sliding and impact wear, Wear 74 (2) (1982) 131–142.

[8] Rice S.L., Nowtony H., Wayne S.F., Formation of subsurface zones in impact wear, Trans. ASME 72 (2) (1982) 264–268

[9] Seif M.A., Abdel-Aal H.A., Temperature fields In dry sliding contact by a hybrid laser-speckle technique, Wear, 181–183 (1995) 723–729

[10] Johns R., Wykes C., Holographic and Speckle Interferometry, Cambridge University Press, Oxford, 1989.

[11] Erf R.K. (Ed.), Speckle Metrology, Academic Press, New York, 1978.

[12] Luxmoore A.R., Amin F.A., Evans W.T., In-plane strain measurements by speckle photography, J. Strain Anal. Eng. 9 (1) (1974) 1–25.

[13] Abdel-Aal H.A., Seif M.A., Thermal strains in nominally flat dry sliding contacts, Mech. Res. Comm. 22 (1) (1995) 59–66.

[14] Post D., Wood J.D., Han B., Parks V.J., Gerstle F.P., Thermal stresses in a bi- material joint: an experimental analysis, ASME J. Appl. Mech. 61 (1989) 192–198.

[15] Post D., Wood J.D., Determination of thermal strains by Moire's interferometry, Experimental Mechanics 29 (1989) 318–322.

[16] Abdel-Aal H.A., Temperature fields in dry sliding contact by a hybrid laser-speckle strain analysis technique, Thesis, Tuskegee University, AL, USA, 1994, also published as, UMI MS 13-57220, Ann Arbor, MI, USA, 1994.

[17] Moslehy F.A, Seif M.A., Rice S.L., Measurement of surface displacements in a tribological contact, Exp. Mech. 30 (1990) 49–55.

[18] Seif M.A., Mohr P.J., Moslehy F.A., Rice S.L., Deformation and strain fields in pin specimens in sliding contact by laser speckle and metallographic techniques, J. Tribol.– T. ASME 112 (1990) 506–512.

[19] Stolz G., Numerical solution to an inverse heat conduction problem, J. Heat Transfer–T. ASME 82 (1960) 20–26.

[20] Beck J.V., Blackwell B., St. Clair C.R., Inverse Heat Conduction Ill-Posed Problems, Wiley Intersciences Publishers, New York, 1985.

[21] Blanc G., Raynaud M., Solution of the inverse heat conduction problem from thermal strain measurements, J. Heat Trans.–T. ASME 118 (1996) 842–849.

[22] Pollock D.D., Physics of Engineering Materials, Prentice Hall, New Jersey, 1992.

[23] Carslaw H.S., Jaeger J.C., Conduction of Heat in Solids, 2nd ed., Oxford University Press, Oxford, 1959.

[24] Shpenkov G. P., Friction Surface Phenomena, Elsevier, Amsterdam, 1995.

[25] Wang Y., Lei T. C., Yan M. F., Gaoc C. Q., Frictional temperature field and its relationship to the transition of wear mechanisms of steel 52100–J. Physics D, Appl. Phys. 25 (1992) A165–A169.

[26] Wang Y., Yan M.F., Xiaodong Li, Ting Qun L., Frictional wear behavior of steel 52100 with different microstructures, J. Tribol.–T. ASME 116 (1992) 255–259.

[27] Bartels R.C.F., Churchill R.V., Resolution of boundary problems by the use of a generalized convolution, Bull. Am. Math. Soc., Series 2 48 (1942) 276–282.

[28] Lim S.C., Ashby M.F., Wear mechanism maps, overview no. 55, Acta Metall. Mater. 35 (1) (1987) 1–24.

[29] Abdel-Aal H.A., Smith S.T., On friction-induced temperatures of rubbing metallic pairs with temperature-dependent thermal properties, Wear 216 (1998) 1–19.

APPENDIX A

Reconstruction of the strain fields from displacement data in DESG analysis

The strain fields associated with the deformations of a solid body may be calculated by means of the so-called '*Lagrangian formulation*'. This strain formulation in terms of displacements is commonly used in solid mechanics, especially if a body undergoes geometric changes, and the deformed shape is to be followed through such distortion. Thus, using the Lagrangian formulation, the total strain components, $\varepsilon_x^{\mathrm{T}}$ and $\varepsilon_y^{\mathrm{T}}$, are expressed in terms of the displacements as:

$$\varepsilon_x^{\mathrm{T}} = \frac{\partial u}{\partial X} + \frac{1}{2}\left[\left(\frac{\partial u}{\partial X}\right)^2 + \left(\frac{\partial v}{\partial X}\right)^2\right] \qquad \text{(A-1)}$$

$$\varepsilon_x^{\mathrm{T}} = \frac{\partial v}{\partial Y} + \frac{1}{2}\left[\left(\frac{\partial u}{\partial Y}\right)^2 + \left(\frac{\partial v}{\partial Y}\right)^2\right] \qquad \text{(A-2)}$$

Applying a discretised version of equations (A–1 and A–2) to the points under analysis, the strain fields within the specimen are recovered from the displacement data. It should be noted that the finite strain components involve only linear and quadratic terms in the components of the displacement gradients. This however is a complete finite-strain tensor and not merely a second order approximation to it.

APPENDIX B

Calculation of the bulk and flash temperature components

B.1. Bulk heating

When a pin specimen slides on a disk, frictional heat is generated at the interface. The heat generated per unit area per second ($J{\cdot}m^{-2}{\cdot}s^{-1}$) is given by:

$$q = \frac{\mu F V}{A_n} \tag{B-1}$$

where μ is the coefficient of friction, F is the normal nominal force on the pin, V is the sliding sped, and A_n is the nominal contact area (area at the end of the pin). A fraction α of the heat diffuses into the pin; the rest goes into the disk. Now, let the mean diffusion distance be L_b. After an initial transient, the temperature in the pin will settle to a quasi-steady state distribution, which can be calculated from the first law of thermodynamics. Linearising the problem, the heat flux ($J{\cdot}m^{-2}s^{-1}$) may be expressed as:

$$J = -K\nabla T \simeq K_m\left[\frac{T_b - T_0}{L_b}\right] \tag{B-2}$$

where K_m is the thermal conductivity, T_b is the bulk surface temperature and T_0 is the sink temperature which may be assumed to be room temperature. Equating this to the incident heat flux αq (using equation B–1), Lim and Ashby [28] obtain the bulk heating as:

$$T_b = T_0 + \frac{\alpha \mu F V L_b}{A_n k_m} \tag{B-3}$$

Equation (B–3) was applied to the experimental conditions of the current work and the bulk heating (thereby the function $f_2(t)$) was determined.

B.2. Flash heating

The temperature produced by injecting an energy density $\alpha q'$ ($J{\cdot}m^{-2}{\cdot}s^{-1}$) into an area πr^2 (the area of an asperity contact) is well approximated by [28]:

$$T_f = T_0 + \frac{\alpha q' r_a}{\pi^{1/2} K_m} \tan^{-1}\left\{\frac{4\,a\,t}{r_a^2}\right\} \tag{B-4}$$

where t is the time of injection, K_m is the thermal conductivity, and α is the fraction of the energy q' which enters the pin. We identify the injection time t with the transit time of an asperity on the pin over one on the disk.

$$t = \frac{2 r_a}{V} \tag{B-5}$$

where V is the sliding velocity. Converting to the dimensionless variables V', T^* gives:

$$T_f = T_0 + \frac{\alpha \mu}{\pi^{1/2} r_0}\frac{r_a}{r_0} T V' \tan^{-1}\left\{\frac{8 r_0}{V' r_a}\right\}^{1/2} \tag{B-6}$$

This expression has two simple limits, one of which is relevant to the present problem. When it is sufficiently large, the arctangent becomes equal to its argument, giving:

$$T_f = T_0 + \frac{\alpha \mu}{\pi^{1/2} r_0}\frac{r_a}{r_0} T V^{1/2}\left\{\frac{2 r_a}{\pi r_0}\right\}^{1/2} \tag{B-7}$$

When, instead, V' is sufficiently small, the arctangent tends to the value $\pi/2$, giving:

$$T_f = T_0 + \frac{1}{2}\pi^{1/2}\alpha \mu T V'\left\{\frac{r_a}{r_0}\right\} \tag{B-6}$$

Equation (B–6) was used to calculate the flash temperature (strength of the temperature pulse in section 6).